atmosphere

MDPI

Article

Dynamics of Precipitation Anomalies in Tropical South America

Mario Córdova [1,2,3,*], Rolando Célleri [1,3] and Aarnout van Delden [2]

[1] Departamento de Recursos Hídricos y Ciencias Ambientales, Universidad de Cuenca, Cuenca 010105, Ecuador; rolando.celleri@ucuenca.edu.ec
[2] Institute for Marine and Atmospheric Research Utrecht (IMAU), Utrecht University, 3508 TA Utrecht, The Netherlands; a.j.vandelden@uu.nl
[3] Facultad de Ingeniería, Universidad de Cuenca, Cuenca 010215, Ecuador
* Correspondence: mario.cordovam@ucuenca.edu.ec

Abstract: In this study, precipitation in Tropical South America in the 1931–2016 period is investigated by means of Principal Component Analysis and composite analysis of circulation fields. The associated dynamics are analyzed using the 20th century ERA-20C reanalysis. It is found that the main climatic processes related to precipitation anomalies in Tropical South America are: (1) the intensity and position of the South Atlantic Convergence Zone (SACZ); (2) El Niño Southern Oscillation (ENSO); (3) the meridional position of the Intertropical Convergence Zone (ITCZ), which is found to be related to Atlantic Sea Surface Temperature (SST) anomalies; and (4) anomalies in the strength of the South American Monsoon System, especially the South American Low-Level Jet (SALLJ). Interestingly, all of the analyzed anomalies are related to processes that operate from the Atlantic Ocean, except for ENSO. Results from the present study are in agreement with the state of the art literature about precipitation anomalies in the region. However, the added strength of the longer dataset and the larger study area improves the knowledge and gives new insights into how climate variability and the resulting dynamics are related to precipitation in Tropical South America.

Keywords: rainfall; tropics; principal component analysis; ENSO; monsoon; SACZ; convergence zone; ERA-20C

Citation: Córdova, M.; Célleri, R.; van Delden, A. Dynamics of Precipitation Anomalies in Tropical South America. *Atmosphere* **2022**, *13*, 972. https://doi.org/10.3390/atmos13060972

Academic Editor: Mario Marcello Miglietta

Received: 27 April 2022
Accepted: 4 June 2022
Published: 15 June 2022

1. Introduction

In Tropical South America, hydrological extremes were more frequent in the last two decades, with a myriad of negative economical, ecological, and societal effects [1,2]. Extreme hydrological events, characterized as "once in a century", were reported in the Amazon region in the past few decades [2]. Precipitation anomalies in the area are related to climate variability, which is complex and influenced by several geographical features, such as the prominent orography of the Andes cordillera, the sea surface temperature (SST) of the Pacific Ocean, the Atlantic Ocean, and the Caribbean Sea. Furthermore, the region is located in both the Southern Hemisphere (SH) and the Northern Hemisphere (NH).

The large variability of precipitation in Tropical South America also results from the superposition of several large-scale phenomena that act on different time scales [3]. The Intertropical Convergence Zone (ITCZ) is the main driver of precipitation seasonality in the region [4]. Over land, the ITCZ is located in the summer hemisphere (on average), but its position over sea and associated precipitation are influenced by SST anomalies [5], which may favor an annual average ITCZ position north of the equator.

A mode of climate variability that widely affects the region is El Niño Southern Oscillation (ENSO). Both its warm (El Niño) and cold (La Niña) phases were linked to positive and negative precipitation anomalies in different regions in Tropical South America [6–14].

A monsoonal circulation is present in Tropical South America, mainly during austral summer [15]. This is so important for precipitation in the region that climatologists describe

the climate of Tropical South America as monsoon-like [3]. The so-called South American Monsoon System (SAMS) is characterized by intense precipitation during the warm season in a region over Central Brazil and Bolivia, which is connected to the Atlantic ITCZ and extends into the South Atlantic Convergence Zone (SACZ). Recent studies have found evidence that the SAMS is changing [16]; and [17] found a reduction of the wet season over the central and southern Andes of Peru. These results suggest a weakening of the SAMS. The South American Low-Level Jet (SALLJ) plays an important role in the SAMS [15,18]. The SALLJ transports moisture southward from the Amazon region along the eastern slopes of the Andes [19], leading to the frequent formation of mesoscale convective systems over the La Plata river basin [20].

Past research, focusing on identifying the causes of extreme drought and flood events in Tropical South America, has linked these extremes to SST variability through climate indices [2,21–23]. Research was also performed to understand the dynamics involved in extreme precipitation and how circulation influences the climatic features in the different sub-regions of Tropical South America [24–28]. Teleconnections play an important role in the region. Extra-tropical processes can influence rainfall in the tropics, which makes it important to consider a larger spatial domain than just the sub-regions. Furthermore, even though it was recognized in the past that processes that vary on decadal or longer time scales are important for precipitation in the region [29], studies usually focus on the relatively short period, 1979 to present, which does not allow for a definitive comprehension of such long-term variability. Therefore, the objective of the present study is to study the teleconnections and dynamics related to precipitation anomalies in Tropical South America over a longer period, using precipitation and circulation data for 1931–2016.

Our paper is structured as follows: Section 2 (Data and Methods) describes the data and methods we used in the present study; Section 3 (Results and Discussion) is devoted to the analysis and discussion of our results, with four subsections, one for each of the first four Principal Components for the Global Precipitation Climatology Centre (GPCC) dataset and their relationship to circulation patterns; finally, Section 4 (Conclusions) summarizes our findings and highlights the new insights obtained because of the temporal and spatial extension of the used dataset.

2. Data and Methods

2.1. Data

The GPCC Full Data Monthly Product Version 2018 at 0.25° resolution is used for monthly precipitation [30]. This is an observation-based gridded dataset for precipitation over land, which covers the period 1891–2016. The rain gauge database used for GPCC has more than 85 thousand stations around the globe. The GPCC has a great capacity to assemble, quality assure, and analyze rain gauge data, the combination of these capacities and their extensive dataset makes it the best possible observational, gridded monthly land surface precipitation dataset worldwide [31]. Furthermore, among the GPCC datasets, the Full Data Monthly Product is the most suitable to analyze the historical global precipitation and teleconnections [30]. From this product, a spatial subset was taken to study precipitation anomalies in Tropical South America. The region of interest is defined within 28° S to 15° N and 85° W to 33° W. The number of stations per grid cell is used to evaluate the reliability of the information over the study area. Before 1931, there were too few stations in the region, mainly over the Amazon and the Andes (Figure S1). Therefore, the study period is limited to 1931–2016. The monthly average precipitation in Tropical South America within each season (i.e., December–January–February (DJF), March–April–May (MAM), June–July–August (JJA), and September–October–November (SON)) for the years, 1931–2016, is shown in Figure 1.

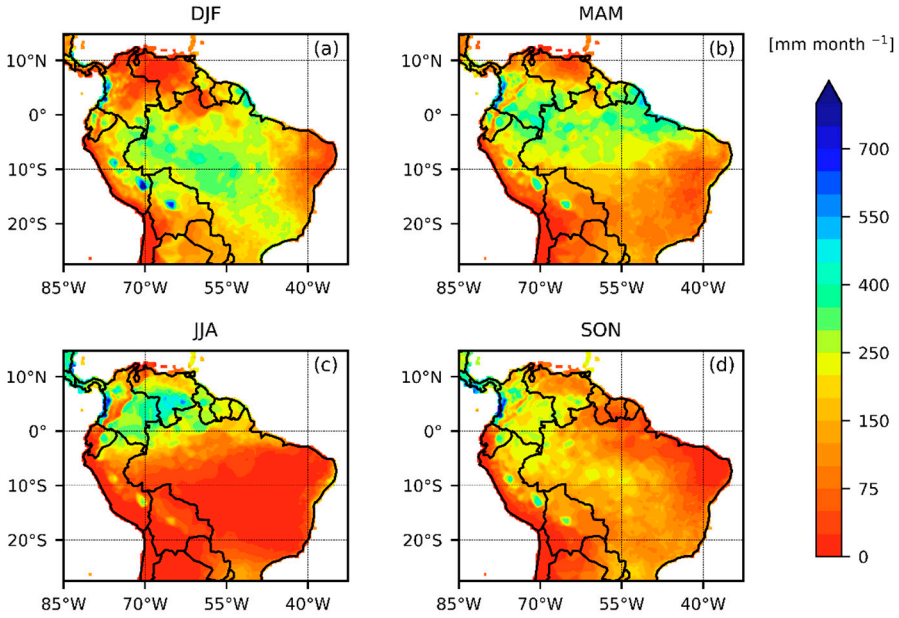

Figure 1. Monthly average precipitation within each season for the 1931–2016 period: (**a**) December–January–February (DJF); (**b**) March–April–May (MAM); (**c**) June–July–August (JJA); and (**d**) September–October–November (SON). Data from the Global Precipitation Climatology Centre (GPCC) Full Data Monthly Product Version 2018 at 0.25° resolution.

To evaluate the relationship between precipitation anomalies and atmospheric dynamics, we used the atmospheric reanalysis of the 20th century, ERA-20C, which runs from 1900 to 2010 [32]. More specifically, we used the monthly means of daily means of zonal wind velocity (u), meridional wind velocity (v), and specific humidity (q), all at 850 hPa, the potential vorticity (PV) at 350 K, the vertical velocity (ω) at 700 hPa, and the vertical integral of divergence of moisture flux (VIDMF). The data were downloaded at 0.25° spatial resolution.

To evaluate teleconnections between precipitation anomalies and SST anomalies, we used the climate indices, Niño 1 + 2 (0°–10° S, 90° W–80° W) and Niño 3.4 (5° N–5° S, 170° W–120° W), for the tropical Pacific SST-anomalies and the Tropical Northern Atlantic (TNA) (25° N–5° N, 55° W–15° W), and the Tropical Southern Atlantic (TSA) (0°–20° S, 30° W–10° W) indices for the tropical Atlantic SST-anomalies. Niño 1 + 2 and Niño 3.4, running from 1870 to the present, are based on the Hadley Centre Sea Ice and Sea Surface Temperature dataset (HadISST1) and are available from the Met Office Hadley Centre [33]. The TNA and TSA indices [34] were calculated from the ERA-20C reanalysis SST-fields for the years 1931–2010. To calculate a SACZ index we used the monthly gridded Outgoing Longwave Radiation (OLR) data, downloaded from the NCEP/National Ocean and Atmospheric Administration (NOAA) [35]. These data have a 2.5° spatial resolution and cover the 1979–2022 period. The method to calculate the SACZ index is described in [36].

2.2. Methods

To extract the leading modes of precipitation variability in Tropical South America, Principal Component Analysis (PCA) was performed on the precipitation data after removing the time–mean yearly (seasonal) cycle. The method consists of calculating the covariance matrix of the deseasonalized precipitation field, and its eigenvalues and eigenvectors. The projection of the precipitation field onto the eigenvectors provides the Principal Component (PC) time series. The spatial patterns, shown in Figure 2, are the spatial representations of the eigenvectors [37]. These maps correspond to the positive phase of the PCs, which shows the pattern of precipitation anomalies in the study area for positive values of each PCA more detailed explanation of the PCA can be found in [38].

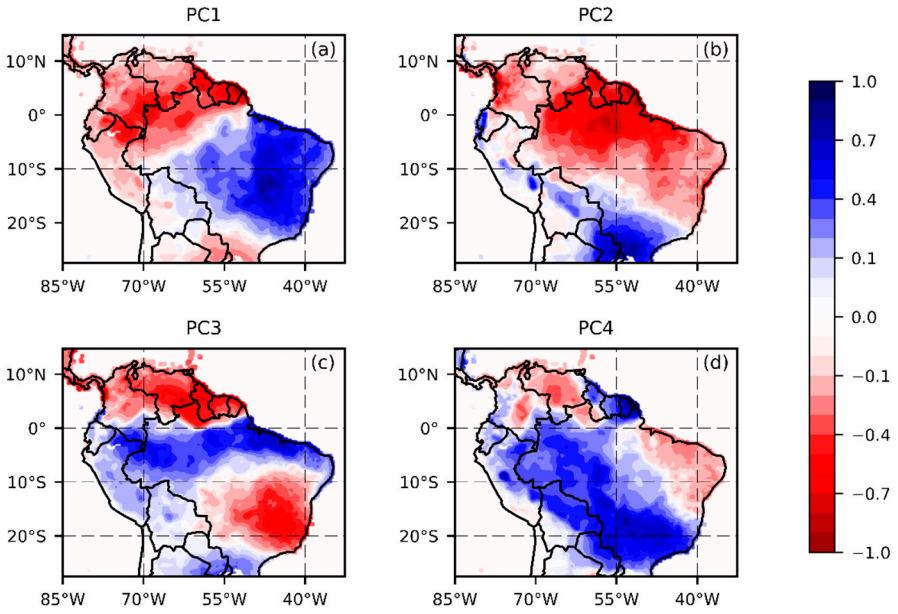

Figure 2. Spatial pattern of the positive phase of the four leading normalized principal components, based on the deseasonalized monthly precipitation from the GPCC dataset for the period 1931–2010. Blue colors are related to positive precipitation anomalies; red colors are related to negative precipitation anomalies. (**a**) PC1, (**b**) PC3, (**c**) PC3, and (**d**) PC4.

To plot the maps corresponding to the PCs, the eigenvectors were normalized (divided by the maximum of the absolute value). This was necessary because annual precipitation varies in a wide range in the region (<100 mm yr^{-1}–>10,000 mm yr^{-1}). The anomalies of the composites of the circulation fields for the 10 years with the maximum and minimum magnitudes of the PC time series were analyzed to determine the spatial patterns related to the precipitation anomalies revealed by the PCs. These anomalies were calculated using 1931–2016 as the base period. Finally, correlations between the PC time series and the climate indices were calculated to determine the role of SST-anomalies on the principal modes of precipitation variability.

3. Results and Discussion

The spatial pattern for the positive phase of the four leading PCs of the deseasonalized precipitation for tropical South America is depicted in Figure 2. These four PCs explain 8.84%, 5.86%, 4.50%, and 3.30% of the total variance in the data. In total, this is 22.5%. This is a large percentage in view of the fact that there are as many PCs as grid cells, i.e., 35,700. Hence, the other 77.5% variance is explained by the remaining 35,696 PCs. Positive values (the blue colors in Figure 2) are related to positive precipitation anomalies, whereas negative values (red colors) are related to negative precipitation anomalies. This section is devoted to determining the circulation patterns and the associated physical mechanisms that explain the anomalies revealed by these four principal components.

3.1. First Principal Component: South Atlantic Convergence Zone (SACZ) Intensity

The positive phase of the first PC displays positive precipitation anomalies over eastern Brazil (20° S–3° S; 50° W–40° W) (Figure 2a). Negative precipitation anomalies are observed close to the equator, in the northern Peruvian Amazon, eastern Colombia, southern Venezuela, Guyana, Suriname, and French Guiana. Positive precipitation anomalies are found roughly in the area affected by the SACZ. The magnitude of the first PC is usually higher in austral summer and fall, when the SACZ is active (Figure 3a). Therefore, it is likely that the first PC is related to anomalies in the SACZ intensity.

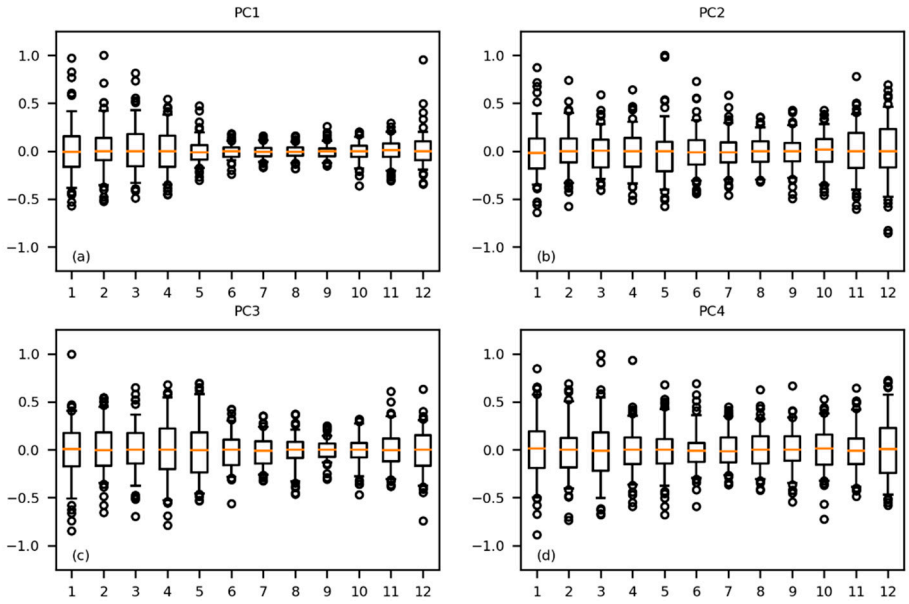

Figure 3. (**a**) Boxplot of the normalized magnitudes of PC1 month by month (horizontal axis); (**b**) Same but for PC2; (**c**) Same but for PC3; (**d**) Same but for PC4.

In a study, using data for Brazil only, [39] found similar precipitation anomalies for the intense mode of the SACZ as the ones shown in Figure 2a, and precipitation anomalies with a similar pattern and opposite sign for the weak mode of the SACZ. In the aforementioned study, it was also found that the intense and weak modes of the SACZ are related, respectively, to westerly and easterly low-level wind anomalies in central South America.

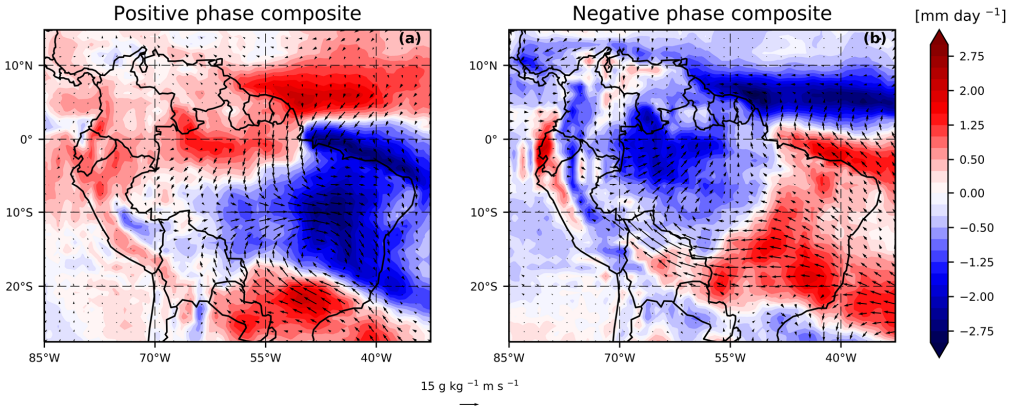

Figure 4. (**a**) DJF anomalies of the composite corresponding to the composite of the 10 years with the maximum magnitude of PC1. Arrows indicate moisture flux at 850 hPa and colors indicate vertical integral of divergence of moisture flux; (**b**) As in (**a**) but for the 10 years with the minimum magnitude of PC1. Note that blue colors indicate moisture flux convergence and red colors indicate moisture flux divergence. Anomalies are defined as the deviation from the average for the period, 1931–2010. Data from ECMWF ERA-20C reanalysis.

Figure 4 shows VIDMF anomalies for the DJF composites for the 10 years with the maximum and minimum magnitudes of PC1. For all of the composites in the present section, strong El Niño events (1982/1983 and 1997/1998) and strong La Niña events (1973/1974 and 2007/2008) are neglected, as they contaminate the analysis. The positive phase shows low-level westward moisture flux anomalies (arrows in Figure 4a), including a cyclonic moisture flux anomaly over Southern Brazil, that are characteristic of the intense mode of the SACZ. The VIDMF anomalies (the shading in Figure 4a) show positive and

negative VIDMF anomalies that match both the precipitation anomaly pattern of the positive phase of PC1, shown in Figure 2a, and the results of [39].

The hypothesis that PC1 is related to the SACZ intensity is also confirmed in Figure 4b, which displays the anomalies for the DJF composites for the 10 years with the minimum magnitudes of PC1. The low-level westward moisture flux anomalies over Eastern Brazil penetrate westward into the region located around the Bolivia-Brazil border; this characterizes the weak mode of the SACZ. A cyclonic moisture flux anomaly is observed over central-west Brazil, centered at 10° S, where positive precipitation anomalies are expected for the weak mode of the SACZ.

Further confirmation of PC1 and its relation to the SACZ intensity was found when the PC1 timeseries was correlated with the OLR-based SACZ index described in Section 2.1. We found a correlation coefficient equal to 0.69.

All of this evidence demonstrates that the pattern shown in Figure 2a is related to the intensity of SACZ, as not only the associated circulation anomalies shown in Figure 4 resemble previously described states of the SACZ, but also the SACZ index is highly correlated to the PC1 timeseries.

Besides the longer record used in the present study, compared to [39], the more extensive study area reveals the effects of the SACZ strength outside Brazil. The intense positive phase is related to precipitation deficits in the northern Peruvian Amazon, eastern Colombia, southern Venezuela, Guyana, Suriname, and French Guiana. The opposite is true for the intense negative phase. Positive precipitation anomalies in relation to the negative phase of PC1 are also observed over southern Paraguay, within the La Plata basin (Figure 2a), where the main source of precipitation is the moisture flux from the Amazon by the SALLJ [40].

In [41], they found that, indeed, the intense mode of SACZ is related to a weaker SALLJ. This is verified in Figure 4a, which shows weak southward moisture flux anomalies over Northern Brazil related to the intense mode of SACZ, while northward moisture flux anomalies over eastern Bolivia and Paraguay indicate a weaker SALLJ, which is associated with less moisture convergence, and hence negative precipitation anomalies over the La Plata river basin. The time series of the first PC is shown in Figure 5a. Extremes of the amplitude of this PC are revealed as spikes and hence have a relatively very short time scale, as variation in the intensity of the SACZ.

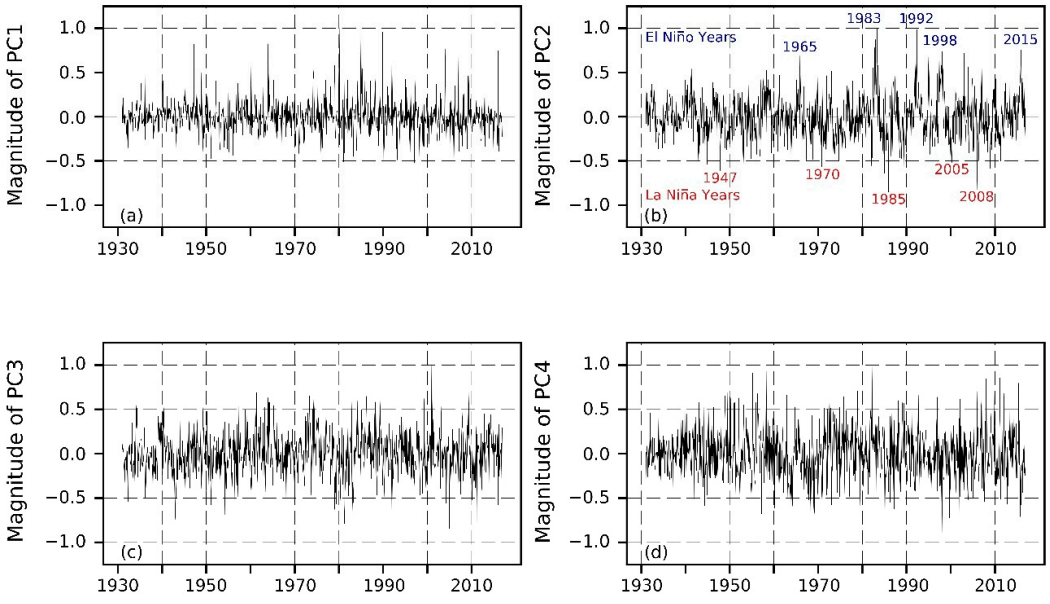

Figure 5. (**a**) Normalized PC1 time series; (**b**) Normalized PC2 time series. Blue labels indicate El Niño events and red labels indicate La Niña events; (**c**) Normalized PC3 time series; (**d**) Normalized PC4 time series. The PC time series is normalized such that the maximum value is +1.

3.2. Second Principal Component: ENSO

The time scale of the extremes of the amplitude of PC1 (Figure 5a) is in contrast to the time scale of the fluctuations of extremes in the amplitude of PC2, shown in Figure 5b. This PC is associated with ENSO, which is characterized by fluctuation in these observed time scales. The correlation coefficient of the amplitude of the second PC with the Niño 3.4 index is 0.49. Extreme positive values of the amplitude of PC2 are associated with El Niño, while extreme negative values are associated with La Niña. The strongest El Niño events of 1982/1983, 1997/1998, and 2015/2016 are easily recognizable in the graph in Figure 5b.

The positive phase of the second PC (Figure 2b) shows positive precipitation anomalies over the coastal plains of Ecuador and Northern Peru, within the La Plata basin in Paraguay, and in southern Brazil and northern Argentina. Negative precipitation anomalies are observed over the northern Amazon basin (in northern Brazil, Guyana, Suriname, and French Guiana), and in the northern coastal region of Colombia. This precipitation anomaly pattern corresponds to known precipitation anomalies associated with El Niño. The negative phase of the second PC corresponds to La Niña, which is associated with anomalies over the same areas as for El Niño, but of an opposite sign; i.e., negative precipitation anomalies over the coastal plains of Ecuador and Northern Peru, positive precipitation anomalies over the northern Amazon basin, and over the northern coastal areas of Colombia.

Indeed, past research has shown that El Niño is related to positive precipitation anomalies in coastal Ecuador and northern Peru [6,7,42,43]. Others [8] have also found a relationship between El Niño and positive precipitation anomalies in the La Plata basin, in relation to an intensification of the subtropical jet stream in the Southern Hemisphere and an increased southward flux of moisture when El Niño conditions prevail [23]. The authors of [11] studied the connection between ENSO and precipitation within the La Plata basin and also found that El Niño is strongly associated with positive precipitation anomalies, centered around the triple border between Paraguay, Argentina, and Brazil, within the La Plata basin (Figure 2b).

El Niño was also associated with drought in the Amazon [2,12] and with negative precipitation anomalies in the Choco region in western Colombia [44]. The latter is explained by the weakening of the Choco low-level jet, the Caribbean low-level jet, and the suppressed convergence of wind over tropical South America [45].

3.3. Third Principal Component—Meridional shift of the Atlantic ITCZ and SACZ

The positive phase of the third PC (Figure 2c) shows negative precipitation anomalies north of the equator and over south-eastern Brazil (10° S–22° S; 50° W–40° W). In between these areas, between the equator and 10° S, over the western Amazon basin, positive precipitation anomalies are observed.

Figure 3c shows that the third PC has the largest amplitude in the wet DJF and MAM seasons. To obtain insight into the dynamics related to this spatial precipitation anomaly pattern, composites of anomalies of VIDMF for DJF and MAM were calculated for the 10 years, with the maximum and minimum magnitudes of the amplitude of PC3 (Figure 6). The anomalies related to the positive phase of PC3 are displayed in Figure 6a,c. Both show a moisture flux convergence-pattern that explains the precipitation anomalies portrayed in Figure 2c. The positive phase of PC3 is characterized by more (less) moisture flux convergence south (north) of the equator. This pattern extends from land to the tropical Atlantic Ocean. The opposite pattern of moisture flux convergence is observed in the negative phase, shown in Figure 6b,d. Especially in DJF, a similar dipolar moisture flux convergence pattern is observed over the area where the SACZ is located (Figure 6a,b).

Based on these results, it is hypothesized that PC3 is related to simultaneous meridional shifts of the ITCZ and the SACZ. In order to test this hypothesis, composites of the zonal average of the vertical velocity, ω, at 700 hPa, between 80° W and 15° W, are constructed for the 10 years with the maximum and minimum magnitudes of the PC3-amplitude. The El Niño and la Niña years are discarded. The composites are calculated for austral fall (MAM), which is the time of the year when the ITCZ migrates from the

Southern to the Northern Hemisphere, and hence anomalies in the meridional position of the convergence zones, especially of the ITCZ, would be most noticeable.

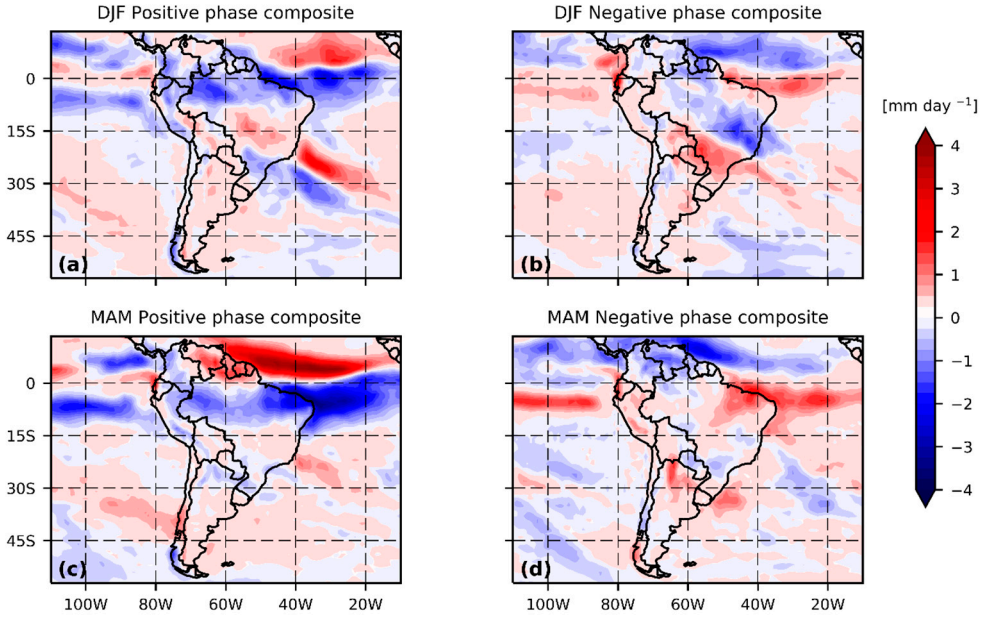

Figure 6. (**a**) DJF anomalies of the vertical integral of divergence of moisture flux corresponding to the composite of the 10 years with the maximum magnitude of PC3; (**b**) As in (**a**) but for the 10 years with the minimum magnitude of PC3; (**c**) MAM Anomalies of the vertical integral of divergence of moisture flux corresponding to the composite of the 10 years with the maximum magnitude of PC3; (**d**) As in (**c**) but for the 10 years with the minimum magnitude of PC3. Note that blue colors are related to more moisture, whereas the red colors indicate the opposite. Anomalies are defined as the deviation from the average for the period, 1931–2010. Data from ECMWF ERA-20C reanalysis.

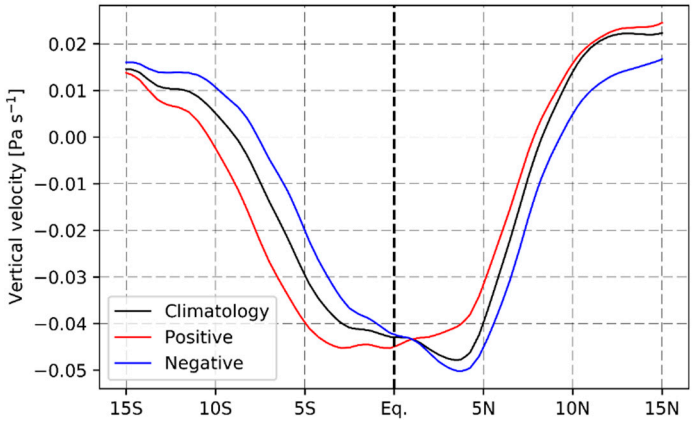

Figure 7. Vertical velocity (ω), the values are zonally averaged in the 80° W–15° W domain. The black line is the MAM climatology. The red and the blue lines are the MAM average for the 10 years with maximum and minimum PC3 amplitude, respectively. Data from ECMWF ERA-20C reanalysis.

Figure 7 shows the composite of ω at 700 hPa for the maximum and the minimum magnitudes of the amplitude of PC3 in MAM, together with the climatology of ω at 700 hPa for the period, 1931–2010. In the climatology (the black line in Figure 7) the position of the ITCZ, which coincides with the minimum value of ω, is located at 4° N. In the positive phase of PC3, the ITCZ is displaced quite far southward into the southern hemisphere. This is consistent with the analysis shown in Figure 2c, where positive precipitation anomalies in the positive phase are located south of the equator. On the other hand, the composite for the negative phase of PC3 reveals a zone of stronger than average upward motion in the

northern hemisphere approximately at the same latitude as in the climatology, which is also consistent with the analysis shown in Figure 2c.

The southward shift of the ITCZ in the positive phase of PC3 is linked to positive SST anomalies in the tropical South Atlantic Ocean [5], especially in the region of the Brazil current, which flows southward along the Brazilian south coast. This is confirmed by the fact that the amplitude of PC3 during MAM correlates positively with TSA, and negatively with TNA. The correlation coefficients are 0.46 and −0.44, respectively.

Negative TNA and positive TSA are also related to a southward shift of the SACZ. This is observed most strongly in austral summer (DJF) (Figure 6a,b), when the SACZ attains its greatest intensity. The authors of [39] found precipitation anomalies in DJF in south-eastern Brazil that resemble the spatial pattern of PC3. These anomalies are characteristic of the so-called "oceanic" and "continental" modes of the SACZ, and are linked to upper-level circulation anomalies.

To analyze the role of upper-level circulation anomalies, we looked at potential vorticity (PV) at the 350 K isentropic level, which intersects the dynamical tropopause in the subtropics. The composite of PV for DJF in the negative phase of PC3 (Figure 8b) shows a cyclonic (negative) PV anomaly centered at 30° S over the South Atlantic Ocean, which weakens the South Atlantic Subtropical High and strengthens the oceanic mode of the SACZ. This agrees with the findings of [39], concerning the oceanic mode of the SACZ, both for precipitation and upper-level circulation anomalies.

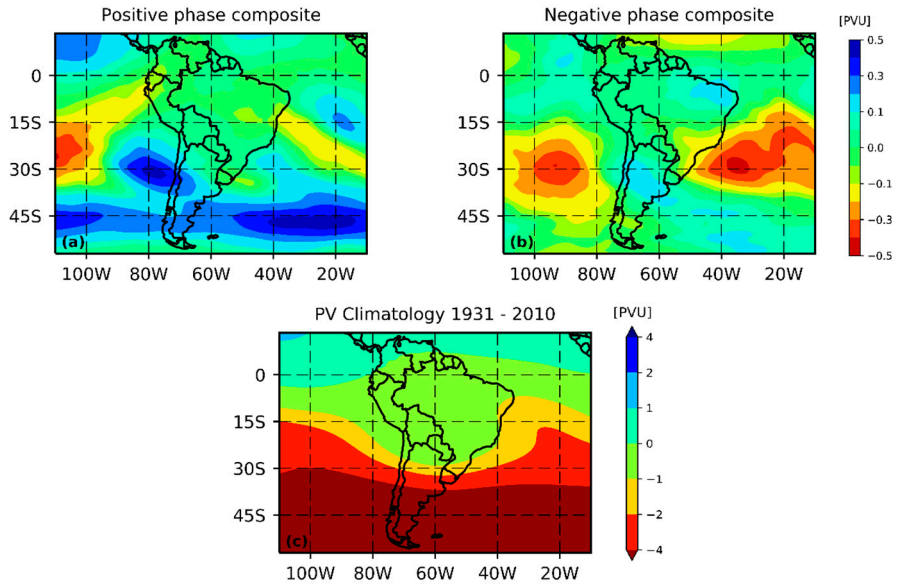

Figure 8. (**a**) DJF Anomalies of potential vorticity corresponding to the composite of the 10 years with the maximum magnitude of PC3; (**b**) As in (**a**) but for the 10 years with the minimum magnitude of PC3; (**c**) PV Climatology for the 1931–2010 period. Data from ECMWF ERA-20C reanalysis.

For the positive phase of PC3 (Figure 8a), the trough is weakened and anomalies are smaller in magnitude. This might be related to the fact that the magnitudes of PC3 are greater for the negative phase than for the positive phase (Figure 3c). Thus, a weaker (stronger) South Atlantic Subtropical High is related to the "oceanic" ("continental") mode of the SACZ, which can be recognized in the stronger (weaker) upper-level trough.

3.4. Fourth Principal Component—South American Monsoon System

The positive phase of the fourth PC shows positive precipitation anomalies in central Brazil and Amazon Bolivia, where the SAMS influences precipitation [46], and negative precipitation anomalies over eastern Brazil, Venezuela, and central Colombia (Figure 2d). The climatology of the 850 hPa moisture flux and VIDMF for austral summer for the 1931–

2010 period is shown in Figure 9c. The easterly Atlantic trade winds, the SALLJ, and the South Pacific and South Atlantic subtropical anticyclones are easily observed.

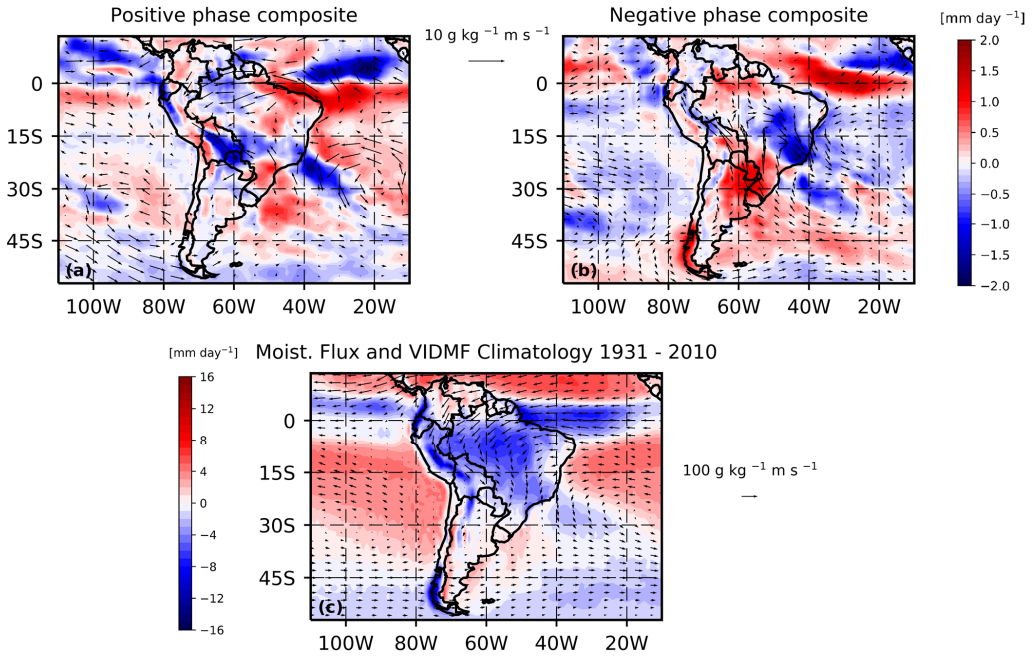

Figure 9. (**a**) DJF Anomalies of 850 hPa moisture flux (arrows) and VIDMF (shading) corresponding to the composite of the 10 years with the maximum magnitude of PC4; (**b**) As in (**a**) but for the 10 years with the minimum magnitude of PC4; (**c**) DJF Climatology of 850 hPa moisture flux (arrows) and VIDMF (shading) for the 1931–2010 period. Data from ECMWF ERA-20C reanalysis.

To detect anomalies in the SAMS related to PC4, anomalies of the composites of 850 hPa wind for the DJF season were calculated for the 10 years with the maximum and minimum magnitudes of PC4 (Figure 9a,b). DJF is analyzed because this is the season when the SAMS is most active.

For the positive phase (Figure 9a), an anomalously strong SAMS is recognized by stronger than average equatorial Atlantic trade winds and stronger than average SALLJ. During the monsoon season, the SALLJ transports moisture to the central Amazon, and to Bolivia and Paraguay. The positive phase of PC4 is also associated with a stronger than average subtropical anticyclone over the South Atlantic. This suggests that the strength of the South Atlantic subtropical anticyclone is correlated to the strength of the SAMS. The stronger South Atlantic anticyclonic might be linked to the negative precipitation anomaly over north eastern Brazil (Figure 2d), through suppressed moisture flux convergence.

The opposite is observed for anomalies related to the negative phase of PC4, i.e., weaker Atlantic trade winds and SALLJ. Suppressed moisture transport is observed especially in the equatorial Atlantic, northern Brazil, and in the area over the La Plata river basin, where the SALLJ brings moisture. In addition, the anticyclonic 850 hPa moisture flux anomaly in the south Atlantic is shifted northward, while a cyclonic 850 hPa moisture flux anomaly is observed just to the south of this anticyclonic anomaly. This spatial pattern explains the precipitation anomalies related to the negative mode of PC4.

4. Conclusions

In this study, precipitation anomalies in Tropical South America for the period, 1931–2016, are investigated. Precipitation anomalies in the region are found to be mainly related to the variability of the South Atlantic Convergence Zone (SACZ), El Niño Southern Oscillation (ENSO), the Inter-Tropical Convergence Zone (ITCZ), and the South American Monsoon System (SAMS). The intense (weak) phase of the SACZ is related to positive (negative) precipitation anomalies in Eastern Brazil and opposite precipitation anomalies

in the Northern Peruvian Amazon, Eastern Colombia, Southern Venezuela, Guyana, Suriname, and French Guiana. Variability in the SACZ position is also related to precipitation anomalies in Eastern Brazil, which are linked to Tropical Atlantic SST anomalies. These anomalies are also connected to the ITCZ position, inducing precipitation anomalies around the equator. El Niño (La Niña) is related to positive (negative) precipitation anomalies in the coastal plains of Ecuador and Northern Peru, and in the La Plata River basin, while opposite precipitation anomalies were found in the Pacific coast of Colombia and the northern area of the Amazon basin. A stronger (weaker) SAMS is related to positive (negative) precipitation anomalies in Guyana, Suriname, French Guiana, the Brazilian Amazon, Eastern Bolivia, and Paraguay and opposite precipitation anomalies in the coastal area of North Eastern Brazil. In the case of the SAMS, results confirmed the hypothesis that recent climate change related to greenhouse gases caused the intensification of the monsoon systems globally [47,48]. However, a clear sign of the intensification of the SAMS is not observed in the PC4 time series (Figure 5d). While it is true that any of the PC time series show a trend over time for our study period (Figure 5), there is an apparent increment in the occurrence and magnitude of extreme amplitudes in the second half of the period (after 1970), especially in PC1 and PC2. This might be related to the observed increment of extreme events caused by the recent anthropogenic climate change.

Results of this study confirm what was found in previous research, but also give new insights about how and which climate variability affects precipitation in the broader region around tropical South America over longer time scales. The much longer period analyzed adds strength to the results of the study of the dynamics related to precipitation anomalies. Additionally, the ERA-20C reanalysis, which, to the knowledge of the authors, was not used in the past for this kind of study in South America, is proven to adequately represent the continental scale dynamics. Finally, the identified physical mechanisms that drive precipitation anomalies and their relation with observed recent climate change and variability could be the base of future forecasting tools for extreme hydrological years in different regions of Tropical South America.

Supplementary Materials: The following supporting information can be downloaded at: https://www.mdpi.com/article/10.3390/atmos13060972/s1, Figure S1: Number of rain gauges in each pixel of the GPCC dataset for different years for the study area. The gray colors correspond to pixels with more than eight rain gauges.

Author Contributions: Conceptualization, M.C. and A.v.D.; methodology, M.C. and A.v.D.; software, M.C.; validation, A.v.D. and R.C.; formal analysis, M.C.; investigation, M.C.; data curation, M.C.; writing—original draft preparation, M.C.; writing—review and editing, A.v.D. and R.C.; visualization, M.C.; supervision, A.v.D. and R.C.; project administration, A.v.D. All authors have read and agreed to the published version of the manuscript.

Funding: This research received no external funding and The APC was funded by Utrecht University.

Institutional Review Board Statement: Not applicable.

Informed Consent Statement: Not applicable.

Data Availability Statement: All data used in this study are publicly available. (1) The Global Precipitation Climatology Centre (GPCC) Full Data Monthly Product Version 2018 at 0.25° is available at https://opendata.dwd.de/climate_environment/GPCC/html/fulldata-monthly_v2018_doi_download.html (accessed on 15 January 2020); (2) The ERA-20C reanalysis is available at https://apps.ecmwf.int/datasets/data/era20c-moda/levtype=sfc/type=an/. Creation of a user profile is needed to download ECMWF datasets (accessed on 15 January 2020); (3) The climate indices are available from NOAA at https://psl.noaa.gov/data/climateindices/list/ (accessed on 15 January 2020); (4) The OLR dataset is available at https://psl.noaa.gov/data/gridded/data.interp_OLR.html (accessed on 20 May 2022).

Acknowledgments: Rolando Célleri and Mario Córdova are grateful to the "High Resolution Radar Analysis of Precipitation Extremes in Ecuador and North Peru and Implications of the Enso Dynamics" project, a collaborating project with the German Research Foundation (Deutsche

Forschungsgemeinschaft-DFG; DFG GZ.: RO3815/2-1) and the Vice-Rectorate for Research of the University of Cuenca (Vicerrectorado de Investigación de la Universidad de Cuenca, VIUC).

Conflicts of Interest: The authors declare no conflict of interest.

References

1. Gagnon, A.S.; Smoyer-Tomic, K.E.; Bush, A.B.G. The El Niño Southern Oscillation and Malaria Epidemics in South America. *Int. J. Biometeorol.* **2002**, *46*, 81–89. [CrossRef]
2. Marengo, J.A.; Espinoza, J.C. Extreme Seasonal Droughts and Floods in Amazonia: Causes, Trends and Impacts. *Int. J. Climatol.* **2016**, *36*, 1033–1050. [CrossRef]
3. Garreaud, R.D.; Vuille, M.; Compagnucci, R.; Marengo, J. Present-Day South American Climate. *Palaeogeogr. Palaeoclimatol. Palaeoecol.* **2009**, *281*, 180–195. [CrossRef]
4. Cerón, W.L.; Kayano, M.T.; Andreoli, R.V.; Avila-Diaz, A.; de Souza, I.P.; Souza, R.A.F. Pacific and Atlantic Multidecadal Variability Relations with the Choco and Caribbean Low-Level Jets during the 1900–2015 Period. *Atmosphere* **2021**, *12*, 1120. [CrossRef]
5. Marshall, J.; Donohoe, A.; Ferreira, D.; McGee, D. The Ocean's Role in Setting the Mean Position of the Inter-Tropical Convergence Zone. *Clim. Dyn.* **2014**, *42*, 1967–1979. [CrossRef]
6. Tobar, V.; Wyseure, G. Seasonal Rainfall Patterns Classification, Relationship to ENSO and Rainfall Trends in Ecuador. *Int. J. Climatol.* **2018**, *38*, 1808–1819. [CrossRef]
7. Sulca, J.; Takahashi, K.; Espinoza, J.C.; Vuille, M.; Lavado-Casimiro, W. Impacts of Different ENSO Flavors and Tropical Pacific Convection Variability (ITCZ, SPCZ) on Austral Summer Rainfall in South America, with a Focus on Peru. *Int. J. Climatol.* **2018**, *38*, 420–435. [CrossRef]
8. Aceituno, P. On the Functioning of Southern Oscillation in the South American Sector Part I: Surface Climate. *Mon. Weather Rev.* **1988**, *116*, 505–524. [CrossRef]
9. Bedoya-Soto, J.M.; Poveda, G.; Trenberth, K.E.; Vélez-Upegui, J.J. Interannual Hydroclimatic Variability and the 2009–2011 Extreme ENSO Phases in Colombia: From Andean Glaciers to Caribbean Lowlands. *Theor. Appl. Climatol.* **2019**, *135*, 1531–1544. [CrossRef]
10. Grimm, A.M.; Tedeschi, R.G. ENSO and Extreme Rainfall Events in South America. *J. Clim.* **2009**, *22*, 1589–1609. [CrossRef]
11. Boulanger, J.P.; Leloup, J.; Penalba, O.; Rusticucci, M.; Lafon, F.; Vargas, W. Observed Precipitation in the Paraná-Plata Hydrological Basin: Long-Term Trends, Extreme Conditions and ENSO Teleconnections. *Clim. Dyn.* **2005**, *24*, 393–413. [CrossRef]
12. Santamaría-Artigas, A.; van der Schrier, G.; Jiménez-Muñoz, J.C.; Barichivich, J.; Sobrino, J.A.; Mattar, C.; Malhi, Y.; Takahashi, K. Record-Breaking Warming and Extreme Drought in the Amazon Rainforest during the Course of El Niño 2015–2016. *Sci. Rep.* **2016**, *6*, 33130. [CrossRef]
13. Bolaños, S.; Salazar, J.F.; Betancur, T.; Werner, M. GRACE Reveals Depletion of Water Storage in Northwestern South America between ENSO Extremes. *J. Hydrol.* **2020**, *596*, 125687. [CrossRef]
14. Cai, W.; McPhaden, M.J.; Grimm, A.M.; Rodrigues, R.R.; Taschetto, A.S.; Garreaud, R.D.; Dewitte, B.; Poveda, G.; Ham, Y.-G.; Santoso, A.; et al. Climate Impacts of the El Niño–Southern Oscillation on South America. *Nat. Rev. Earth Environ.* **2020**, *1*, 215–231. [CrossRef]
15. Rodrigues, M.A.M.; Garcia, S.R.; Kayano, M.T.; Calheiros, A.J.P.; Andreoli, R.V. Onset and Demise Dates of the Rainy Season in the South American Monsoon Region: A Cluster Analysis Result. *Int. J. Climatol.* **2021**, *42*, 1354–1368. [CrossRef]
16. Giráldez, L.; Silva, Y.; Zubieta, R.; Sulca, J. Change of the Rainfall Seasonality Over Central Peruvian Andes: Onset, End, Duration and Its Relationship With Large-Scale Atmospheric Circulation. *Climate* **2020**, *8*, 23. [CrossRef]
17. Imfeld, N.; Sedlmeier, K.; Gubler, S.; Correa Marrou, K.; Davila, C.P.; Huerta, A.; Lavado-Casimiro, W.; Rohrer, M.; Scherrer, S.C.; Schwierz, C. A Combined View on Precipitation and Temperature Climatology and Trends in the Southern Andes of Peru. *Int. J. Climatol.* **2021**, *41*, 679–698. [CrossRef]
18. Liebmann, B.; Mechoso, C.R. The South American Monsoon System. In *The Global Monsoon System: Research and Forecast*; Chang, C.-P., Ed.; World Scientific: Singapore, 2011; pp. 137–157, ISBN 978-981-4460-68-2.
19. Silva Dias, M.A.; Emmanuel, C.B.; Nicolini, M.; Meitin, J.; Penalba, O.; Dias, P.S.; Douglas, M.; Paegle, J.; Saulo, C.; Baez, J.; et al. The South American Low-Level Jet Experiment. *Bull. Am. Meteorol. Soc.* **2006**, *87*, 63–78. [CrossRef]
20. Salio, P.; Nicolini, M.; Zipser, E.J. Mesoscale Convective Systems over Southeastern South America and Their Relationship with the South American Low-Level Jet. *Mon. Weather Rev.* **2007**, *135*, 1290–1309. [CrossRef]
21. Campozano, L.; Trachte, K.; Célleri, R.; Samaniego, E.; Bendix, J.; Albuja, C.; Mejia, J.F. Climatology and Teleconnections of Mesoscale Convective Systems in an Andean Basin in Southern Ecuador: The Case of the Paute Basin. *Adv. Meteorol.* **2018**, *2018*, 4259191. [CrossRef] [PubMed]
22. Vuille, M.; Bradley, R.; Keimig, F. Climate Variability in the Andes of Ecuador and Its Relation to Tropical Pacific and Atlantic Sea Surface Temperature Anomalies. *J. Clim.* **2000**, *13*, 2520–2535. [CrossRef]
23. Grimm, A.M.; Barros, V.R.; Moira, E.D. Climate Variability in Southern South America Associated with El Niño and La Niña Events. *J. Clim.* **2000**, *13*, 35–58. [CrossRef]
24. Espinoza, J.C.; Ronchail, J.; Marengo, J.A.; Segura, H. Contrasting North–South Changes in Amazon Wet-Day and Dry-Day Frequency and Related Atmospheric Features (1981–2017). *Clim. Dyn.* **2018**, *52*, 5413–5430. [CrossRef]

25. Paccini, L.; Espinoza, J.C.; Ronchail, J.; Segura, H. Intra-Seasonal Rainfall Variability in the Amazon Basin Related to Large-Scale Circulation Patterns: A Focus on Western Amazon–Andes Transition Region. *Int. J. Climatol.* **2018**, *38*, 2386–2399. [CrossRef]
26. Cavalcanti, I.F.A.; Carril, A.F.; Penalba, O.C.; Grimm, A.M.; Menéndez, C.G.; Sanchez, E.; Cherchi, A.; Sörensson, A.; Robledo, F.; Rivera, J.; et al. Precipitation Extremes over La Plata Basin—Review and New Results from Observations and Climate Simulations. *J. Hydrol.* **2015**, *523*, 211–230. [CrossRef]
27. Cavalcanti, I.F.A. Large Scale and Synoptic Features Associated with Extreme Precipitation over South America: A Review and Case Studies for the First Decade of the 21st Century. *Atmos. Res.* **2012**, *118*, 27–40. [CrossRef]
28. Mendoza, D.E.; Samaniego, E.P.; Mora, D.E.; Espinoza, M.J.; Campozano, L.V. Finding Teleconnections from Decomposed Rainfall Signals Using Dynamic Harmonic Regressions: A Tropical Andean Case Study. *Clim. Dyn.* **2018**, *52*, 4643–4670. [CrossRef]
29. Segura, H.; Espinoza, J.C.; Junquas, C.; Takahashi, K. Evidencing Decadal and Interdecadal Hydroclimatic Variability over the Central Andes. *Environ. Res. Lett.* **2016**, *11*, 094016. [CrossRef]
30. Schneider, U.; Becker, A.; Finger, P.; Anja, M.-C.; Ziese, M. GPCC Full Data Monthly Product Version 2018 at 0.25°: Monthly Land-Surface Precipitation from Rain-Gauges Built on GTS-Based and Historical Data. 2018. Available online: https://www.dante-project.org/datasets/gpcc (accessed on 15 January 2020).
31. Becker, A.; Finger, P.; Meyer-Christoffer, A.; Rudolf, B.; Schamm, K.; Schneider, U.; Ziese, M. A Description of the Global Land-Surface Precipitation Data Products of the Global Precipitation Climatology Centre with Sample Applications Including Centennial (Trend) Analysis from 1901−Present. *Earth Syst. Sci. Data* **2013**, *5*, 71–99. [CrossRef]
32. Poli, P.; Hersbach, H.; Dee, D.P.; Berrisford, P.; Simmons, A.J.; Vitart, F.; Laloyaux, P.; Tan, D.G.H.; Peubey, C.; Thépaut, J.N.; et al. ERA-20C: An Atmospheric Reanalysis of the Twentieth Century. *J. Clim.* **2016**, *29*, 4083–4097. [CrossRef]
33. Rayner, N.A.; Parker, D.E.; Horton, E.B.; Folland, C.K.; Alexander, L.V.; Rowell, D.P.; Kent, E.C.; Kaplan, A. Global Analyses of Sea Surface Temperature, Sea Ice, and Night Marine Air Temperature since the Late Nineteenth Century. *J. Geophys. Res.* **2003**, *108*, 4407. [CrossRef]
34. Enfield, D.B.; Mestas-Nuñez, A.M.; Mayer, D.A.; Cid-Serrano, L. How Ubiquitous Is the Dipole Relationship in Tropical Atlantic Sea Surface Temperatures? *J. Geophys. Res. Ocean.* **1999**, *104*, 7841–7848. [CrossRef]
35. Liebmann, B.; Smith, C.A. Description of a Complete (Interpolated) Outgoing Longwave Radiation Dataset. *Bull. Am. Meteorol. Soc.* **1996**, *77*, 1275–1277.
36. Sulca, J.C.; Rocha, R.P. Influence of the Coupling South Atlantic Convergence Zone-El Niño-Southern Oscillation (SACZ-ENSO) on the Projected Precipitation Changes over the Central Andes. *Climate* **2021**, *9*, 77. [CrossRef]
37. Raziei, T.; Bordi, I.; Pereira, L.S. An Application of GPCC and NCEP/NCAR Datasets for Drought Variability Analysis in Iran. *Water Resour. Manag.* **2011**, *25*, 1075–1086. [CrossRef]
38. Rencher, A.C. *Multivariate Statistical Inference and Applications*; John Wiley & Sons, Inc.: Hoboken, NJ, USA, 1998.
39. Carvalho, L.M.V.; Jones, C.; Liebmann, B. The South Atlantic Convergence Zone: Intensity, Form, Persistence, and Relationships with Intraseasonal to Interannual Activity and Extreme Rainfall. *J. Clim.* **2004**, *17*, 88–108. [CrossRef]
40. Wang, M.; Paegle, J. Impact of Analysis Uncertainty upon Regional Atmospheric Moisture Flux. *J. Geophys. Res.* **1996**, *101*, 7291–7303. [CrossRef]
41. Robertson, A.W.; Mechoso, C.R. Interannual and Interdecadal Variability of the South Atlantic Convergence Zone. *Mon. Weather Rev.* **2002**, *128*, 2947–2957. [CrossRef]
42. Bendix, A.; Bendix, J. Heavy Rainfall Episodes in Ecuador during El Niño Events and Associated Regional Atmospheric Circulation and SST Patterns. *Adv. Geosci.* **2006**, *6*, 43–49. [CrossRef]
43. Dijkstra, H. *Nonlinear Physical Oceanography*, 2nd ed.; Springer: Dordrecht, The Netherlands, 2005; ISBN 140202262X.
44. Poveda, G.; Mesa, Ó.J. Las Fases Extremas Del Fenómeno ENSO (El Niño y La Niña) y Su Influencia Sobre La Hidrología de Colombia. *Ing. Hidráulica Méximo* **1996**, *XI*, 21–37. Available online: http://www.revistatyca.org.mx/ojs/index.php/tyca/article/view/765/726 (accessed on 23 May 2022).
45. Poveda, G.; Mesa, Ó.J. La Corriente de Chorro Superficial Del Oeste ("de Chocó") y Otras Dos Corrientes de Chorro En Colombia: Climatología y Variabilidad Durante Las Fases Del Enso. *Rev. Acad. Colomb. Ciencias* **1999**, *23*, 517–528.
46. Mechoso, C.R.; Robertson, A.W.; Ropelewski, C.F.; Grimm, A.M. The American Monsoon Systems. In Proceedings of the 3rd International Workshop on Monsoons, Hangzhou, China, 2–6 November 2004.
47. Hsu, P.C.; Li, T.; Wang, B. Trends in Global Monsoon Area and Precipitation over the Past 30 Years. *Geophys. Res. Lett.* **2011**, *38*, 1–5. [CrossRef]
48. Véspoli De Carvalho, L.M.; Charles, J. *The Monsoons and Climate Change: Observations and Modeling*, 1st ed.; Springer: Berlin/Heidelberg, Germany, 2016; ISBN 9783319216492.